Four Direction Residual Interpolation for Demosaicking

Yonghoon Kim and Jechang Jeong

***Abstract*— In this paper, we propose a four direction residual interpolation method for color filter array interpolation. The proposed algorithm exploits a guided filtering process to generate the tentative image. The residual image is generated by exploiting the tentative and original images. We use a four direction residual interpolation algorithm to more accurately estimate the missing pixel values; the estimated image is adaptively combined with a joint inverse gradient weight. Based on experimental results, the proposed method provides superior performance in terms of objective and subjective quality compared to conventional state-of-the-art demosaicking methods.**

***Index Terms*—Bayer pattern, color filter array (CFA) interpolation, demosaicking, residual interpolation, directional interpolation.**

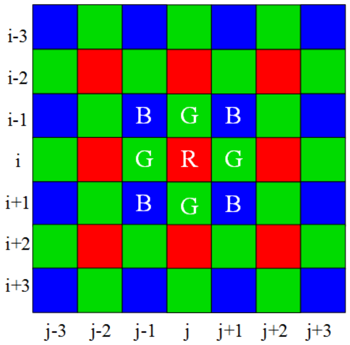

Fig. 1. Bayer color filter array.

I. Introduction

MOST image data uses the RGB color format, which contains red, green, and blue data for each pixel position. A typical digital camera employs a single sensor covered with a color filter array (CFA); therefore, it captures all three color channels, but one at each pixel position. Using the obtained pixels, missing color pixels must be interpolated to create a complete color image. This process of generating a full color image from the subsampled color image is called color filter array interpolation or demosaicking.

The most common CFA pattern is the Bayer pattern [1], shown in Fig. 1. Half of the pixels of the Bayer pattern are allocated to the green channel because it is more useful for representing detail and is less affected by aliasing. The key characteristic of the Bayer pattern is that each color pixel is aligned at a regular distance, which abets accurate interpolation using the correlation between color channels. The reconstruction process of the three-color components is called CFA interpolation or demosaicking [2]. The simplest method of generating missing pixels is to separately fill the missing pixels of each channel using a bilinear or bicubic interpolation algorithm, which is a spatially invariant interpolation method. These algorithms typically show good results in the homogenous region; however, they produce artifacts, such as aliasing or blurring, at the texture and edge structure.

In the past few years, many demosaicking algorithms have been proposed to enhance interpolation performance and image quality. To preserve edge and texture, an edge-directed interpolation method generates the missing color components along the estimated interpolation directions by exploiting the spectral correlation of neighboring color components [3-13]. Zhang *et al.* [4] proposed directional linear minimum mean square error estimation (DLMMSE), which uses a soft direction decision. It optimally combines color differences along horizontal and vertical directions. In [7], Paliy *et al.* suggest a directional approach with scale-adaptive filtering based on local polynomial approximation (LPA). The authors of [8]-[10] separately calculate vertical and horizontal gradients of red and blue channels, which they use as correction terms to improve the green channel interpolation. In [11], Menon *et al.* used color gradients over a local window for directional filtering with an a posteriori decision. In addition, a new approach has been proposed based on the finding that refinement of the green channel yields a higher quality image. Pekkucuksen *et al.* proposed an orientation-free edge strength filter (ESF) [12] and multiscale gradient (MSG)-based color filter array interpolation [13]. Both algorithms utilize an accumulated gradient to calculate the weight for vertical and horizontal directions; moreover, they more accurately estimate edge direction and more efficiently use edge calculation [13] to non-iteratively update the green channel.

In [14], Li *et al.* report on the test dataset. They claim that the Kodak dataset [15] is not suitable for the test because its images acquired by digital cameras of an earlier period have different characteristics than those of today, whereas the McMaster

"This research was supported by the MSIP(Ministry of Science, ICT & Future Planning), Korea, under the project for technical development of information communication & broadcasting supervised by IITP (Institute for Information & Communications Technology Promotion)(IITP 2015-B0101-15-1377)

Y. Kim is with the Department of Electronics and Computer Engineering, Hanyang University, Haengdangdong, Sungdonggu, Seoul, South Korea (e-mail: charismakyh@gmail.com).

J. Jeong is with the Department of Electronics and Computer Engineering, Hanyang University, Haengdangdong, Sungdonggu, Seoul, South Korea (corresponding author, e-mail: jjeong@hanyang.ac.kr).

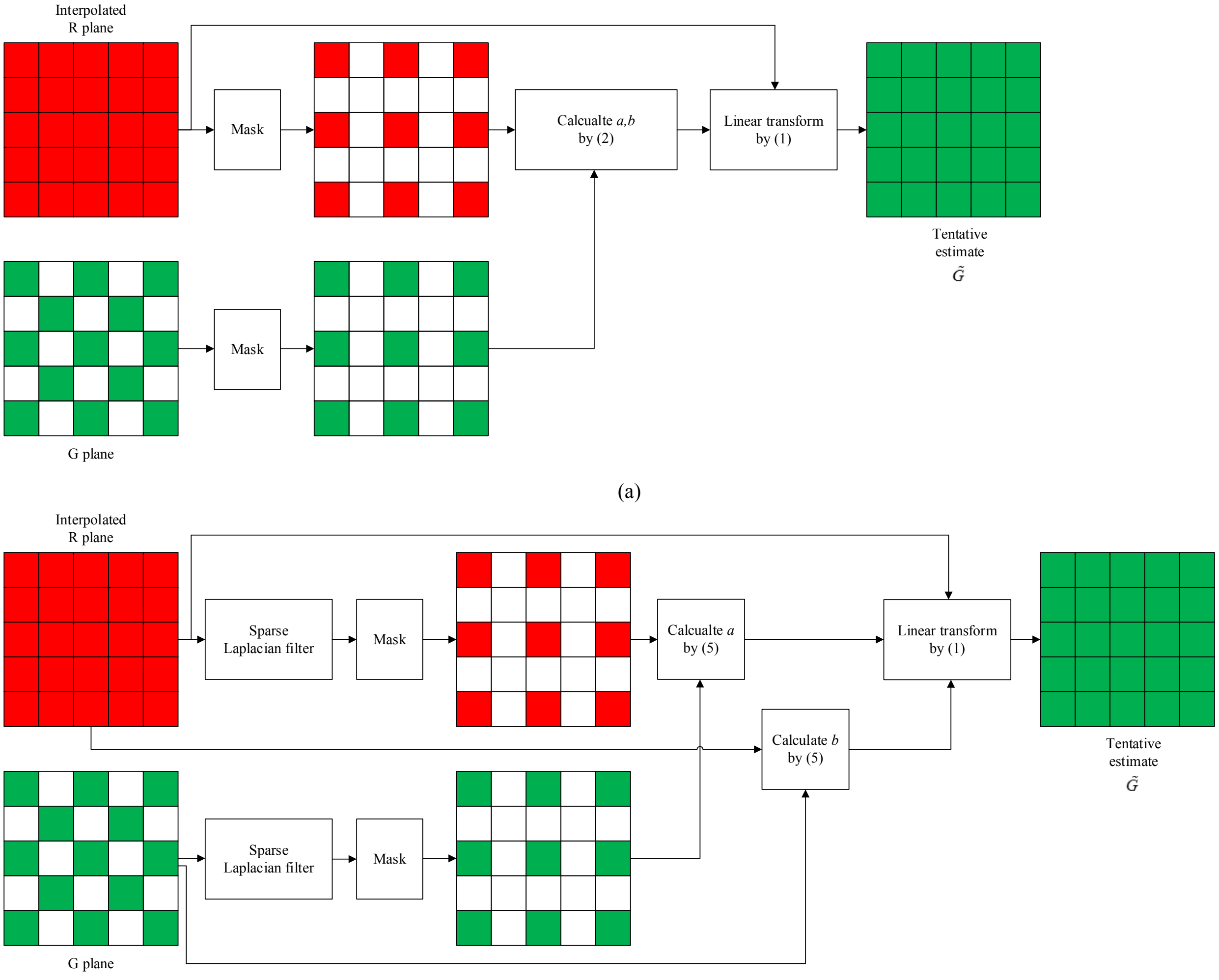

(a)

(b)

Fig. 2. Outline of the guided upsampling process of (a) RI and (b) MLRI.

dataset contains images that are more similar to current images. From that point, several algorithms have been proposed that focus on characteristics of the new dataset [16-20]. Zhang *et al.* proposed the local directional interpolation and nonlocal adaptive thresholding (LDI-NAT) algorithm [16], which shows good performance on the McMaster dataset but has very high complexity. In [18], the author aims to adopt voting-based directional interpolation (VDI). In [19] and [20], residual interpolation (RI) techniques are introduced. The RI method exploits characteristics of the guided filter [22] and shows significant performance improvement. However, these recently proposed VDI [18], RI [19], and minimized Laplacian RI (MLRI) [20] methods still produce severe demosaicking artifacts.

In this paper, we propose a four direction residual interpolation algorithm (FDRI), which is based on RI techniques. The remainder of this paper is structured as follows. In Section II, the concepts of RI and MLRI are given, and the proposed FDRI is introduced in Section III. The performance evaluation of the proposed algorithm is given in Section IV, and Section V reports the conclusion.

II. Related Work

The proposed algorithm is based on the RI [19] and MLRI [20] algorithms. The guided filtering technique is exploited to calculate the residual data. The guided filter is a powerful edge-preserving filter and filter and has lower complexity than the bilateral filter; however, it provides better behavior near edges than the bilateral filter. Both filters require two reference images: input image *q* and guidance image *I*. The guided filter calculates filtering output $\tilde{q}$ by considering the characteristics of guidance image *I*, which itself can be the input image or a different image [22]. The guided filter derives the linear model from the guidance image and target image. The linear model is given as follows:

$$q_i = a_k I_{i,} + b_k, \forall i \in \omega_k, \tag{1}$$

where a_k and b_k denote the linear coefficients assumed to be constant in local window ω_k. To determine the coefficients, the cost function in the window is given as:

$$E(a_k, b_k) = \sum_{i\in\omega_k} (a_k I_{i,} + b_k - q_i)^2, \tag{2}$$

and the solution is given as:

$$a_k = \frac{\frac{1}{|\omega|}\sum_{i\in\omega_k} I_i q_i - \mu_k \bar{q}_k}{\sigma_k^2}, \qquad \mathrm{b_k} = \bar{q}_k - a_k \mu_k, \tag{3}$$

where μ_k and σ_k^2 are the mean and variance of I in ω_k, $|\omega|$ is the number of pixels in ω_k, and $\bar{q}_k$ is the mean of q in ω_k. (1) is not identical when it is computed in different windows. The simple solution is to average the coefficients as follows:

$$\tilde{q}_i = \bar{a}_k I_{i,} + \bar{b}_k, \tag{4}$$

where $\bar{a}_k$ and $\bar{b}$ respectively denote the average coefficients of a_k and b_k in ω_k, and $\tilde{q}_i$ is the filtered output. The guided filter can be used for denoising, dehazing, and guided feathering. Furthermore, it can be applied in the demosaicking area because it can transfer the structures of the guidance image to the filtering output. There have been several attempts to derive the color correlation in the demosaicking field using a guided filter. The first attempt was proposed in [20]. The RI exploits the guided filter to calculate the missing pixels using a different color plane as input image q and guidance image I; the filtering output is called the tentative image.

To improve RI estimation performance, the use of minimized Laplacian RI (MLRI) is proposed. The motivation for using MLRI is that bilinear interpolation can provide better interpolation performance for images that have smaller Laplacian energies. To calculate coefficient a, Laplacian filtered input q^{Lap} and guidance image I^{Lap} are exploited, and b is calculated using original q and I. Therefore, (3) is rewritten as

$$a_k = \frac{\frac{1}{|\omega|}\sum_{i\in\omega_k} I_i^{Lap} q_i^{Lap} - \mu_k^{Lap}\bar{q}_k^{Lap}}{(\sigma_k^{Lap})^2}, \qquad \mathrm{b_k} = \bar{q}_k - a_k \mu_k, \tag{5}$$

where μ_k^{Lap} and $(\sigma_k^{Lap})^2$ are the mean and variance of I^{Lap} in ω_k, $|\omega|$ is the number of pixels in ω_k, and $\bar{q}_k^{Lap}$ is the mean of q^{Lap} in ω_k.

TABLE I
SPARSE LAPLACIAN FILTER EXPLOITED IN MLRI AND THE PROPOSED ALGORITHM.

	MLRI	Proposed algorithm
Green channel interpolation (horizontal)	$\begin{pmatrix}1 & 0 & -2 & 0 & 1\end{pmatrix}$	$\begin{pmatrix}1&0&1&0&1\\0&0&0&0&0\\1&0&-8&0&1\\0&0&0&0&0\\1&0&1&0&1\end{pmatrix}$
Green channel interpolation (vertical)	$\begin{pmatrix}1\\0\\-2\\0\\1\end{pmatrix}$	
Red and blue channel interpolation	$\begin{pmatrix}0&0&1&0&0\\0&0&0&0&0\\1&0&-4&0&1\\0&0&0&0&0\\0&0&1&0&0\end{pmatrix}$	$\begin{pmatrix}1&0&1&0&1\\0&0&0&0&0\\1&0&-8&0&1\\0&0&0&0&0\\1&0&1&0&1\end{pmatrix}$

The outline of the RI and MLRI processes are given in Fig. 2. As shown in fig.2 (a) and (b), to obtain the guided filtered G image, original G image and interpolated R image are required because R pixels do not exist at G pixel location. To interpolate R pixels at G pixel position, 2-tap bilinear filter ([1/2 1/2]) is used. Using the output tentative image, the missing pixel is estimated by exploiting the difference, which is residual, between the originally captured G value and tentative estimates $\tilde{G}$. If $\tilde{G}^H$ is the horizontal tentative estimate of the G pixel at the R pixel position, then the target G pixel value is estimated as follows:

$$G_{i,j}^H = \tilde{G}_{i,j}^H + \frac{(G_{i,j-1} - \tilde{G}_{i,j-1}^H) + (G_{i,j+1} - \tilde{G}_{i,j+1}^H)}{2} \tag{6}$$

where G^H denotes the horizontal estimate of G. In the vertical case, it is given as:

$$G_{i,j}^V = \tilde{G}_{i,j}^V + \frac{(G_{i,j-1} - \tilde{G}_{i,j-1}^V) + (G_{i,j+1} - \tilde{G}_{i,j+1}^V)}{2} \tag{7}$$

where G^V denotes the vertical estimates of G, and $\tilde{G}^V$ is the vertical tentative estimate of G. Using the residuals of vertical and horizontal neighbors, the target value is estimated; these directional estimates are adaptively combined using directional weight. This method provides significant objective quality improvement; nevertheless, subjective quality remains insufficient. To solve this problem, we change the structure of the residual interpolation process and it will be discussed next section.

III. PROPOSED ALGORITHM

The proposed FDRI algorithm exploits the four direction residual interpolation algorithm for the missing G pixel. The proposed algorithm requires only a tentative G plane, whereas RI and MLRI require tentative G, R, and B planes for the G channel interpolation. The proposed algorithm interpolates the G plane using an estimated G and originally captured G plane; however, RI and MLRI utilize the vertical and horizontal color differences of G-R and G-B for directional estimation. The guided filtering processes of the proposed algorithm, RI, and MLIR are shown in Fig. 3. As shown in the figure, the guided filtering value of the proposed algorithm is half of what RI and MLRI require for G channel interpolation.

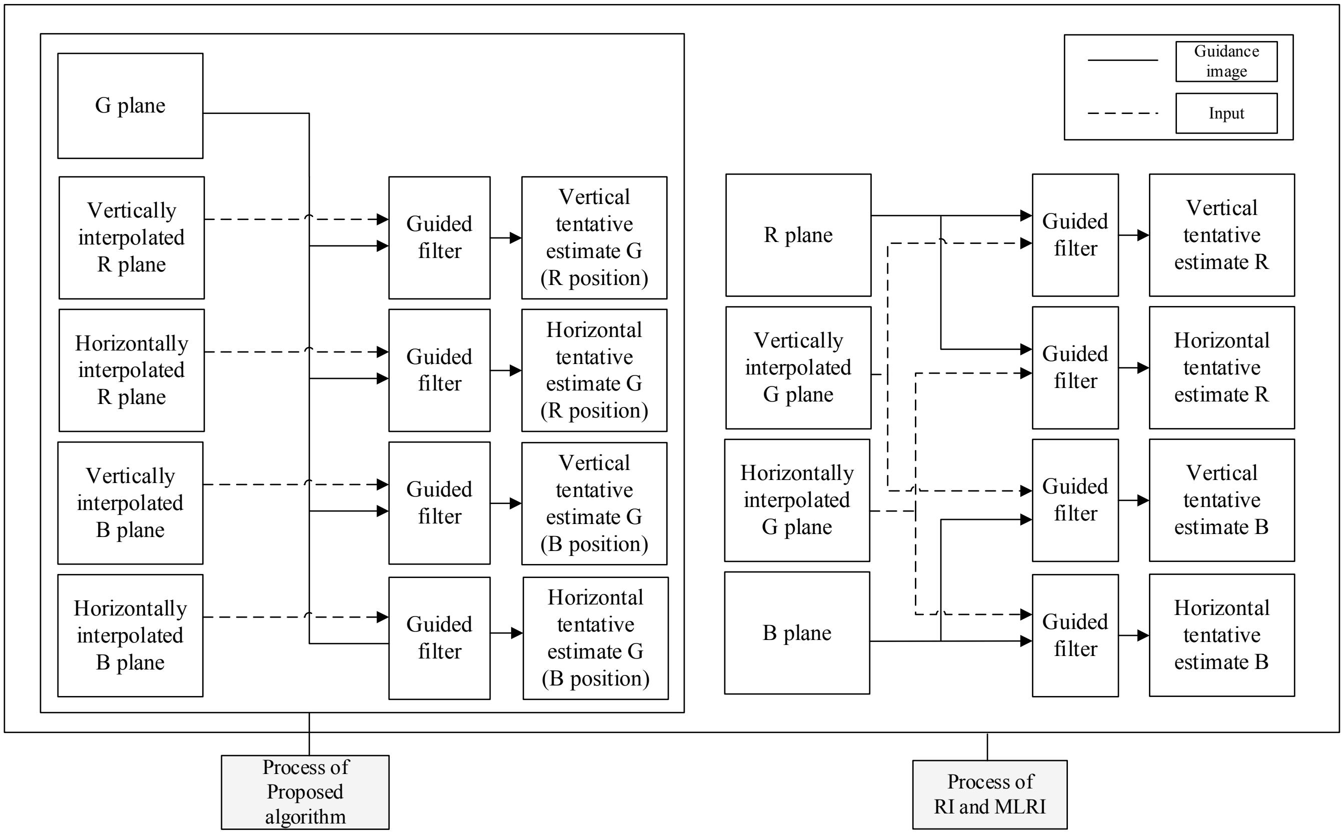
G plane
Vertically interpolated R plane
Horizontally interpolated R plane
Vertically interpolated B plane
Horizontally interpolated B plane
Guided filter
Guided filter
Guided filter
Guided filter
Vertical tentative estimate G (R position)
Horizontal tentative estimate G (R position)
Vertical tentative estimate G (B position)
Horizontal tentative estimate G (B position)
Guidance image
Input
R plane
Vertically interpolated G plane
Horizontally interpolated G plane
B plane
Guided filter
Guided filter
Guided filter
Guided filter
Vertical tentative estimate R
Horizontal tentative estimate R
Vertical tentative estimate B
Horizontal tentative estimate B
Process of Proposed algorithm
Process of RI and MLRI

Fig. 3. Guided filtering process required for *G* plan interpolation of proposed algorithm, RI, and MLRI.

To improve the guided filtering process, we use a different Laplacian filter with MLRI; it is shown in Table I. We determined that the 5x5 Laplacian filter, which considers diagonal neighbors, gives better estimation performance than the 1D directional Laplacian filter used in MLRI.

A. Four Directional Weights using Joint Gradient

In this paper, we use four directional interpolation. To more accurately combine directional estimates, we derive the gradient from two intra channels: the original Bayer pattern plane (Z) and the horizontally and vertically interpolated Bayer plane (Z^H, Z^V). The directionally interpolated Bayer plane is given as follows:

$$\begin{aligned} Z^H &= Z * f, \\ Z^V &= Z * f^T, \end{aligned} \tag{8}$$

where $f = [1/4, 1/2, -1/2, 1/2, 1/4]$, which is Hamilton and Adams' interpolation filter [21]. The directional gradients are given as:

$$\begin{aligned} \Delta^H(i,j) &= \left|Z_{i,j-1} - Z_{i,j+1}\right| + \left|Z^H_{i,j+1} - Z^H_{i,j-1}\right|, \\ \Delta^V(i,j) &= \left|Z_{i-1,j} - Z_{i+1,j}\right| + \left|Z^V_{i-1,j} - Z^V_{i+1,j}\right|, \end{aligned} \tag{9}$$

where Δ^H and Δ^V represent the joint gradients of horizontal and vertical directions, respectively. In the Bayer pattern plane, only one gradient can be calculated at a pixel position. However, using the interpolated Bayer plane, we can obtain a gradient of a different color plane at the same pixel position. The directional weights are made by inversing the local sum of gradients. Using (9), the four directional weights are calculated as:

$$\begin{aligned} w^N_{i,j} &= \sum_{a=-1}^{1}\sum_{b=-1}^{1} \Delta^V(i-1+a, j+b), \\ w^S_{i,j} &= \sum_{a=-1}^{1}\sum_{b=-1}^{1} \Delta^V(i+1+a, j+b), \\ w^E_{i,j} &= \sum_{a=-1}^{1}\sum_{b=-1}^{1} \Delta^H(i+a, j-1+b), \\ w^W_{i,j} &= \sum_{a=-1}^{1}\sum_{b=-1}^{1} \Delta^H(i+a, j+1+b), \end{aligned} \tag{10}$$

where $w^N_{i,\mathrm{j}}$, $w^S_{i,\mathrm{j}}$, $w^E_{i,\mathrm{j}}$, and $w^W_{i,\mathrm{j}}$ denote the weights of north, south, east, and west, respectively.

B. Green Channel Interpolation

Using the process represented in Fig. 2(b), we obtain the vertical and horizontal tentative images. Using the tentative images, we estimate the *G* value in the four directions. The proposed four direction residual interpolation is given as follows:

$$\begin{cases} G^N_{i,j} = \tilde{G}^V_{i,j} - (\tilde{G}^V_{i-1,j} - G_{i-1,j}) \\ G^S_{i,j} = \tilde{G}^V_{i,j} - (\tilde{G}^V_{i+1,j} - G_{i+1,j}) \\ G^E_{i,j} = \tilde{G}^H_{i,j} - (\tilde{G}^H_{i,j-1} - G_{i,j-1}) \\ G^W_{i,j} = \tilde{G}^H_{i,j} - (\tilde{G}^H_{i,j+1} - G_{i,j+1}) \end{cases}, \tag{11}$$

where $G^N_{i,j}$, $G^S_{i,j}$, $G^E_{i,j}$, and $G^W_{i,j}$ denote directional estimates of

This article has been accepted for publication in a future issue of this journal, but has not been fully edited. Content may change prior to final publication. Citation information: DOI 10.1109/TCSVT.2015.2428552, IEEE Transactions on Circuits and Systems for Video Technology

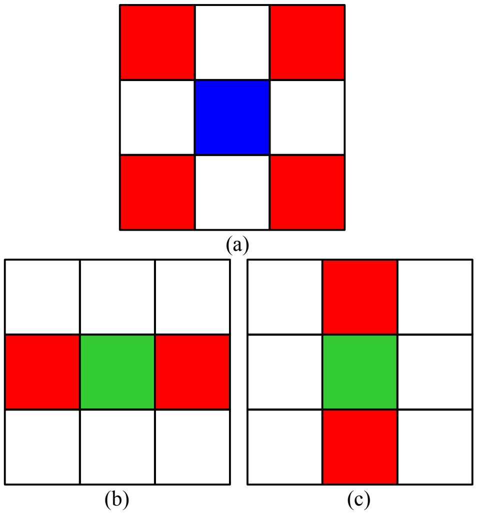

Fig. 4. Three different available reference pixels based on pixel position for red pixel interpolation: (a) diagonal, (b) horizontal, and (c) vertical.

G in the north, south, east, and west directions, respectively. These values and the original G values are adaptively combined using the weight in (10) as:

$$G' = \alpha \times (w_{i,\mathrm{j}}^{N} G_{i,j}^{N} + w_{i,\mathrm{j}}^{S} G_{i,j}^{S} + w_{i,\mathrm{j}}^{E} G_{i,j}^{E} + w_{i,\mathrm{j}}^{W} G_{i,j}^{W}) + (1-\alpha) \times (w_{i,\mathrm{j}}^{N} G_{i-1,j} + w_{i,\mathrm{j}}^{S} G_{i+1,j} + w_{i,\mathrm{j}}^{E} G_{i,j-1} + w_{i,\mathrm{j}}^{W} G_{i,j+1}), \tag{12}$$

where G' represents the reconstructed G pixel and α is experimentally determined as 0.7. We expected this combination to be more accurate than the combination without the original pixel because the original G pixel can correct the misguided estimates.

C. Red and Blue Channel Interpolation

After the G pixels are fully reconstructed, the R and B planes are interpolated using a similar method to the G plane interpolation. For the R plane, the reconstructed G plane can be the input image, and the R plane serves as the guidance image. At this stage, we do not apply a directional weight. The residual is given as follows:

$$\Gamma(i,j) = \tilde{R}(i,j) - R(i,j), \tag{13}$$

where $\tilde{R}$ is the tentative estimates of R, and Γ denotes the residual. These residual data can be combined based on pixel position, as shown in Fig. 4. At the B pixel position in Fig. 4(a), only diagonal references are available; therefore, the interpolation process of R is given as:

$$R'(i,j) = \tilde{R}(i,j) - \frac{\Gamma(i-1,j-1)+\Gamma(i-1,j+1)+\Gamma(i+1,j-1)+\Gamma(i+1,j+1)}{4}, \tag{14}$$

where R' is the reconstructed R pixel. The interpolation processes of R at the G pixel position are calculated as:

Fig. 5. 18 McMaster test images.

$$R'(i,j) = \tilde{R}(i,j) - \frac{\Gamma(i,j-1)+\Gamma(i,j+1)}{2}, \tag{15}$$

$$R'(i,j) = \tilde{R}(i,j) - \frac{\Gamma(i-1,j)+\Gamma(i+1,j)}{2}. \tag{16}$$

Equation (15) is exploited for the horizontal case in Fig. 4(b); (16) is exploited for the vertical case in Fig. 4(c). The interpolation process for the missing B pixels can be achieved in the same method by exchanging the roles of R and B, as explained above. After the interpolation process, we obtain the full three color images.

IV. Experimental Results

To evaluate the performance of the proposed algorithm, we tested it on 18 McMaster dataset images [23] with a resolution of 500x500, as listed in Fig. 5. We chose the McMaster dataset because the images have lower spectral correlations and are similar to nature images captured by color sensors. The widely used Kodak dataset is outdated because the images are scanned from film-based photographs and their characteristics do not match those of current images [14]. Therefore, the Kodak dataset was not suitable for a fair demosaicking performance comparison. The proposed FDRI algorithm was compared with ESF [12], DLMMSE [9], MSG [13], LPA [7], effective demosaicking algorithm based on edge property (EDAEP) [17], VDI [18], LDI-NAT [16], RI [19], and MLRI [20].

To simulate the proposed algorithm, we conducted experiments using MATLAB with an Intel Core i7-4770k and 3.5 GHz CPU processer. To avoid the boundary effects, every calculation excluded the border of ten pixels around the image. The numerical results are summarized in Table II for each of the 18 test images. The results are in ascending order of average CPSNR value; the highest CPSNR value is in bold. The S-CIELAB results, which show perceptual color fidelity, are given in Table III; its lowest value is likewise in bold. It measures how close the reconstructed color is to the original color when viewed by a human observer [23]. To further evaluate the performance of the proposed method, we adopted another measure, the feature similarity index for image quality assessment (FSIMc) [25]. This model considers image distortion, such as gradient correlation, luminance distortion, and contrast distortion; when the value of FSIMc is close to 1, the reconstructed image is similar to the original image. In Table

TABLE II
CPSNR COMPARISON WITH 18 MCMASTER IMAGES (dB).

No.	ESF	DLMMSE	MSG	LPA	EDAEP	VDI	LDI-NAT	RI	MLRI	FDRI
1	26.38	26.98	27.05	26.82	27.60	28.01	29.01	29.12	28.97	**29.38**
2	33.48	33.68	33.67	33.84	33.99	34.18	35.01	35.00	35.08	**35.16**
3	32.56	32.59	32.93	32.47	32.07	32.64	32.56	33.75	**33.86**	33.54
4	34.97	34.32	35.49	34.94	34.36	36.00	35.94	37.86	37.64	**38.06**
5	30.64	31.27	31.12	31.39	32.10	32.63	34.09	33.91	33.99	**34.83**
6	32.57	33.84	33.56	34.37	35.03	35.63	37.87	38.29	38.26	**38.91**
7	39.10	38.64	39.17	**39.20**	36.22	36.03	35.96	36.95	37.46	35.85
8	37.85	37.45	37.61	37.88	37.12	37.41	37.46	36.96	36.94	**38.17**
9	34.39	34.41	34.69	35.07	35.23	35.95	36.91	35.92	36.44	**37.54**
10	35.78	36.34	36.47	37.02	37.01	37.28	38.72	38.15	38.62	**39.02**
11	36.61	37.25	37.28	37.72	37.83	37.98	39.48	39.43	39.91	**40.02**
12	36.16	36.60	36.80	36.97	37.16	37.09	38.89	39.61	39.64	**39.95**
13	38.67	38.79	38.83	39.29	39.34	39.40	40.78	40.27	40.51	**41.01**
14	37.21	37.23	37.13	37.54	37.65	37.32	38.67	38.92	38.76	**39.32**
15	37.01	37.27	37.19	37.66	37.76	37.86	38.93	38.37	38.91	**39.45**
16	29.24	30.46	30.18	29.48	31.39	31.40	33.52	35.17	35.09	**35.42**
17	28.57	29.31	29.30	29.27	30.59	31.15	32.83	32.44	32.58	**33.76**
18	33.69	33.92	34.10	33.96	34.05	34.23	35.00	**36.52**	36.12	36.21
average	34.16	34.46	34.59	34.72	34.81	35.12	36.20	36.48	36.60	**36.98**

TABLE III
S-CIELAB COMPARISON WITH 18 MCMASTER IMAGES.

No.	ESF	DLMMSE	MSG	LPA	EDAEP	VDI	LDI-NAT	RI	MLRI	FDRI
1	3.784	3.204	3.170	3.414	2.903	2.620	2.495	2.486	2.517	**2.381**
2	1.453	1.315	1.252	1.267	1.246	1.144	1.087	1.016	1.035	**0.987**
3	2.076	2.083	1.825	2.103	2.290	1.893	1.854	1.592	1.621	**1.468**
4	1.461	1.443	1.086	1.169	1.484	1.113	1.000	**0.661**	0.781	0.723
5	1.771	1.615	1.551	1.518	1.526	1.374	1.222	1.158	1.165	**1.100**
6	1.857	1.511	1.502	1.410	1.278	1.127	0.965	0.898	0.910	**0.832**
7	0.944	0.941	**0.897**	0.877	1.228	1.199	1.173	1.119	1.076	1.229
8	0.659	0.631	0.589	0.584	0.723	0.613	0.586	0.578	0.575	**0.565**
9	1.396	1.377	1.203	1.199	1.305	1.058	0.964	0.976	1.006	**0.871**
10	1.192	1.083	1.025	0.968	0.999	0.932	0.837	0.838	0.795	**0.768**
11	0.907	0.793	0.783	0.745	0.725	0.675	0.604	0.624	0.611	**0.582**
12	1.257	1.089	1.081	1.057	0.940	0.956	0.824	0.746	0.731	**0.727**
13	0.739	0.711	0.692	0.667	0.683	0.650	0.582	0.577	0.579	**0.559**
14	0.860	0.797	0.784	0.758	0.789	0.742	0.691	0.664	0.680	**0.644**
15	0.913	0.855	0.836	0.807	0.819	0.773	0.719	0.745	0.719	**0.676**
16	2.839	2.064	2.317	2.594	1.673	1.499	1.391	1.365	1.383	**1.365**
17	3.090	2.826	2.577	2.757	2.290	1.960	1.826	1.797	1.827	**1.521**
18	1.601	1.510	1.460	1.506	1.451	1.287	1.234	**1.063**	1.168	1.138
average	1.600	1.436	1.368	1.411	1.353	1.201	1.114	1.050	1.065	**1.008**

IV, the values closest to 1 are marked in bold.

As shown by information in Table II, the proposed algorithm outperformed the other algorithms on 15 out of 18 images. Its average CPSNR was higher than the closest method (MLRI) by 0.38 dB and RI by 0.50 dB. The S-CIELAB measure likewise showed similar results, as presented in Table III. The proposed method outperformed the other methods on 15 out of 18 images. It is remarkable that MLRI gave a lower performance than RI in terms of the S-CIELAB measure despite it having has higher average CPSNR performance. However, the proposed algorithm, which uses the same guided filtering method as MLRI, was superior to RI. This indicates that the proposed four direction residual approach is effective and robust for a demosaicking application.

To further evaluate the performance of the proposed method, we computed the FSIMc values for each of the compared methods using the McMaster image dataset. The results are outlined in Table IV. In terms of FSIMc, the proposed FDRI demonstrated the best performance, and LDI-NAT gave the second best performance. In terms of individual images, FDRI outperformed the other algorithms on 10 out of 18 images; LDI-NAT outperformed the other methods on 5 out of 18 images.

To compare subjective quality, Figs. 6 to 8 illustrate the partially zoomed images: Image 1, Image 5, and Image 17. As shown in Fig. 6, the proposed algorithm greatly improved interpolation performance. The shirt region of Image 5 is shown in Fig. 7; the proposed algorithm perfectly removed the false coloring artifact. Our strategy of exploiting joint weight and flexible interpolation techniques has the advantage of removing demosaicking artifacts. Fig. 8 additionally shows that the proposed algorithm outperformed the other algorithms, and LDI-NAT gave a fair performance. From the subjective results, ESF, LPA, and MSG, which were focused on the Kodak dataset, showed significant quality degradation. VDI, RI, and MLRI gave good CPSNR results; however, they showed relatively lower subjective image quality. Aside from FDRI, the other

TABLE IV
FSIMC COMPARISON WITH 18 MCMASTER IMAGES.

No.	ESF	DLMMSE	MSG	LPA	EDAEP	VDI	LDI-NAT	RI	MLRI	FDRI
1	0.9906	0.9938	0.9924	0.9918	0.9927	0.9935	**0.9956**	0.9952	0.9954	0.9955
2	0.9959	0.9970	0.9964	0.9966	0.9966	0.9968	0.9977	0.9976	0.9976	**0.9977**
3	0.9973	0.9986	0.9978	0.9975	0.9970	0.9975	0.9986	0.9989	**0.9990**	0.9988
4	0.9985	0.9992	0.9988	0.9986	0.9982	0.9987	0.9993	0.9995	0.9996	**0.9996**
5	0.9960	0.9974	0.9967	0.9969	0.9971	0.9974	0.9986	0.9986	0.9986	**0.9987**
6	0.9971	0.9986	0.9980	0.9983	0.9984	0.9985	**0.9993**	0.9991	0.9992	0.9992
7	0.9987	**0.9990**	0.9989	0.9988	0.9978	0.9978	0.9984	0.9988	0.9989	0.9985
8	0.9978	0.9981	0.9979	0.9981	0.9979	0.9981	0.9985	0.9976	0.9976	**0.9987**
9	0.9968	0.9975	0.9973	0.9976	0.9976	0.9978	0.9986	0.9976	0.9981	**0.9986**
10	0.9981	0.9984	0.9985	0.9986	0.9984	0.9985	0.9991	0.9988	0.9990	**0.9991**
11	0.9980	0.9984	0.9984	0.9985	0.9984	0.9984	**0.9991**	0.9986	0.9989	0.9990
12	0.9981	0.9985	0.9984	0.9985	0.9984	0.9983	0.9990	0.9991	0.9991	**0.9992**
13	0.9977	0.9982	0.9979	0.9982	0.9983	0.9983	0.9989	0.9989	0.9989	**0.9991**
14	0.9977	0.9983	0.9980	0.9982	0.9983	0.9985	0.9989	0.9988	0.9988	**0.9990**
15	0.9977	0.9980	0.9980	0.9981	0.9980	0.9981	0.9985	0.9979	0.9984	**0.9985**
16	0.9955	0.9979	0.9969	0.9961	0.9977	0.9977	**0.9987**	0.9986	0.9985	0.9986
17	0.9937	0.9959	0.9952	0.9949	0.9958	0.9958	**0.9979**	0.9966	0.9973	0.9975
18	0.9976	0.9983	0.9979	0.9978	0.9977	0.9980	0.9985	**0.9989**	0.9988	0.9988
average	0.9968	0.9980	0.9974	0.9974	0.9975	0.9977	0.9985	0.9983	0.9984	**0.9986**

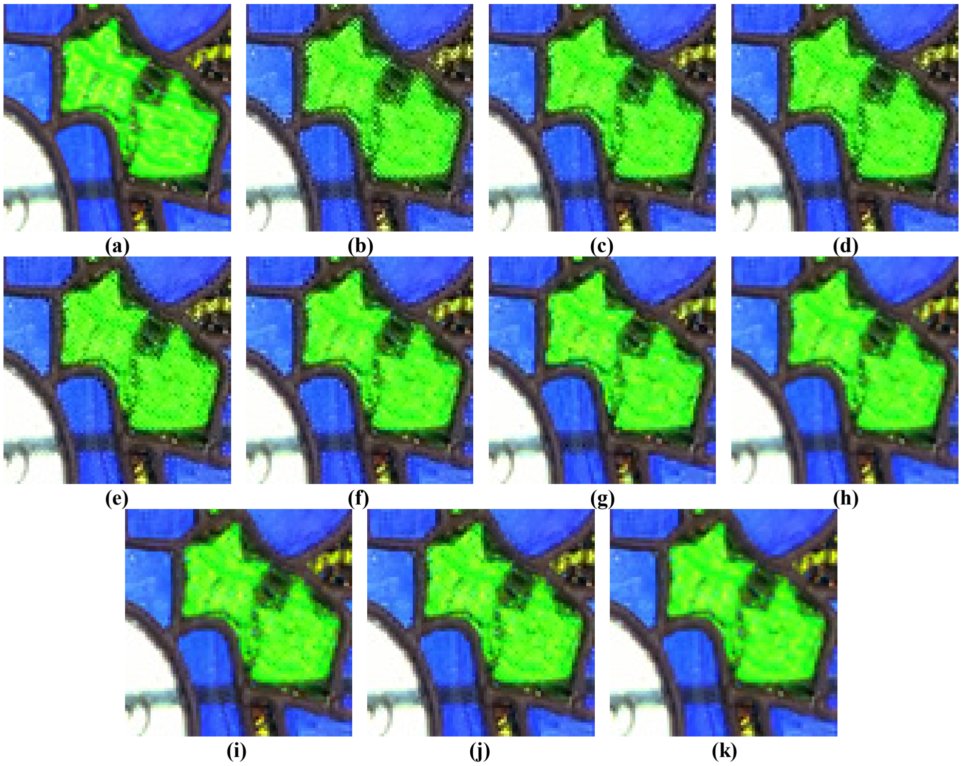

Fig. 6. Demosaicking results of a cropped region of Image 1: (a) original image, (b) ESF, (c) DLMMSE, (d) MSG, (e) LPA, (f) EDAEP, (g) VDI, (h) LDI-NAT, (i) RI, (j) MLRI, and (k) FDRI.

algorithms showed various demosaicking artifacts. It is evident that the proposed four direction residual interpolation strategy successfully worked and produced clean images without demosaicking artifacts.

To further evaluation, we tested demosaicking algorithms on two images included in LC images which are captured using Cannon digital camera [26]. The subjective results are shown in Fig. 9 and 10. In Fig. 9, the proposed FDRI gives the best results without any demosaicking artifacts. ESF, DLMMSE, MSG, and LPA give the severe demosaicking artifact, and EDAEP, VDI, LDI-NAT, RI and MLRI show relatively small artifacts but they are still noticeable. As shown in Fig. 10, most demosaicking algorithms show severe artifacts at the boundary and they cannot interpolate the diagonal edge properly, however FDRI shows few demosaicking artifacts and clearly generate diagonal edge.

TABLE V
COMPLEXITY COMPARISON OF RI, MLRI, AND FDRI.

	RI	MLRI	FDRI
Guided filtering (*G* channel interpolation)	8	8	4
Guided filtering (*R* and *B* channel interpolation)	2	2	2
Laplacian filtering	0	18	8
Residual calculation	10	10	6

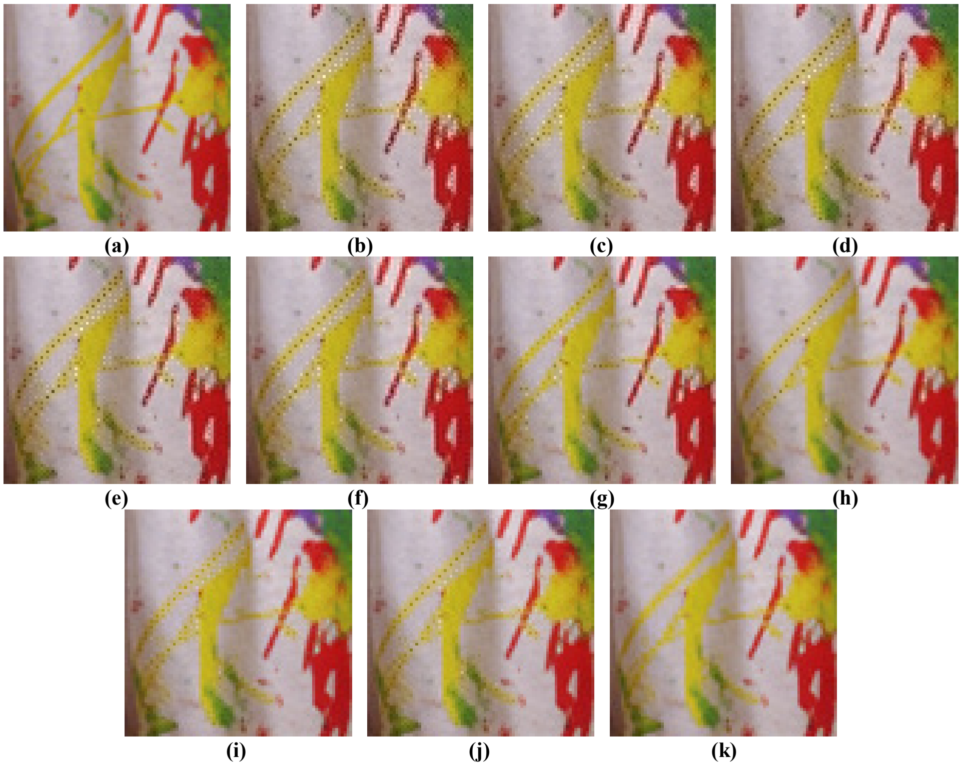

Fig. 7. Demosaicking results of a cropped region of Image 5: (a) original image, (b) ESF, (c) DLMMSE, (d) MSG, (e) LPA, (f) EDAEP, (g) VDI, (h) LDI-NAT, (i) RI, (j) MLRI, and (k) FDRI.

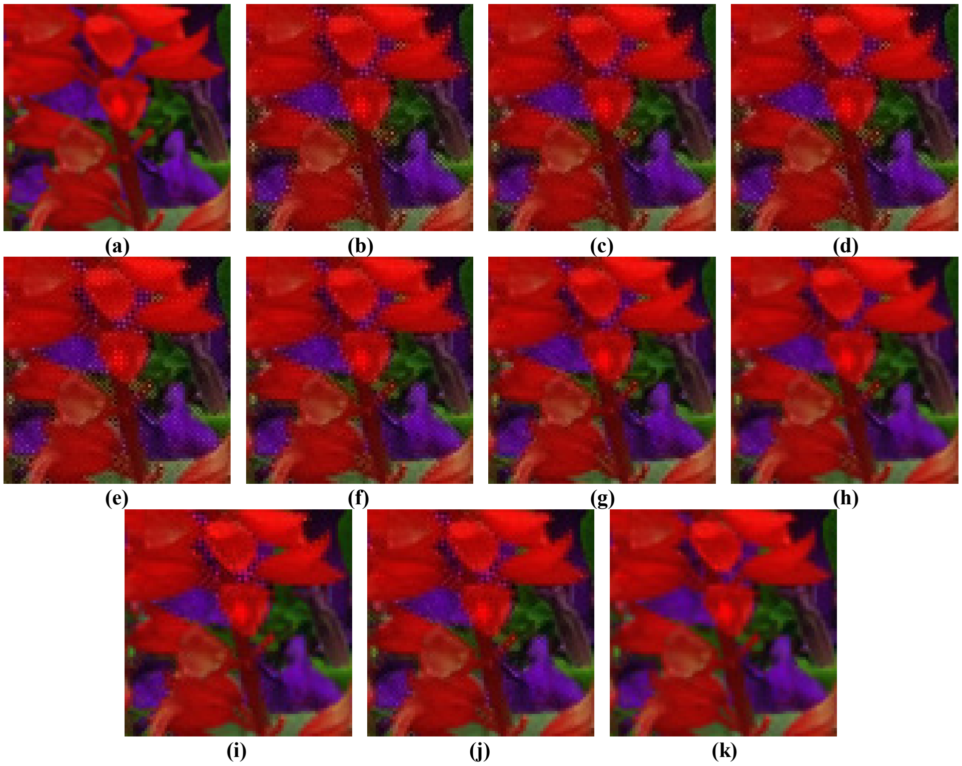

Fig. 8. Demosaicking results of a cropped region of Image 17: (a) original image, (b) ESF, (c) DLMMSE, (d) MSG, (e) LPA, (f) EDAEP, (g) VDI, (h) LDI-NAT, (i) RI, (j) MLRI, and (k) FDRI.

The numbers of required processes of RI, MLRI, and FDRI are shown in Table V. For guided filtering, residual calculating, and Laplacian filtering, the numbers of required processes per one image are listed. We represented only filtering and residual calculation processes because the operations of other processes, such as weight calculating and combining directional estimates, are very similar for RI, MLRI, and FDRI. Guided filtering was the most time-consuming process. FDRI required half the

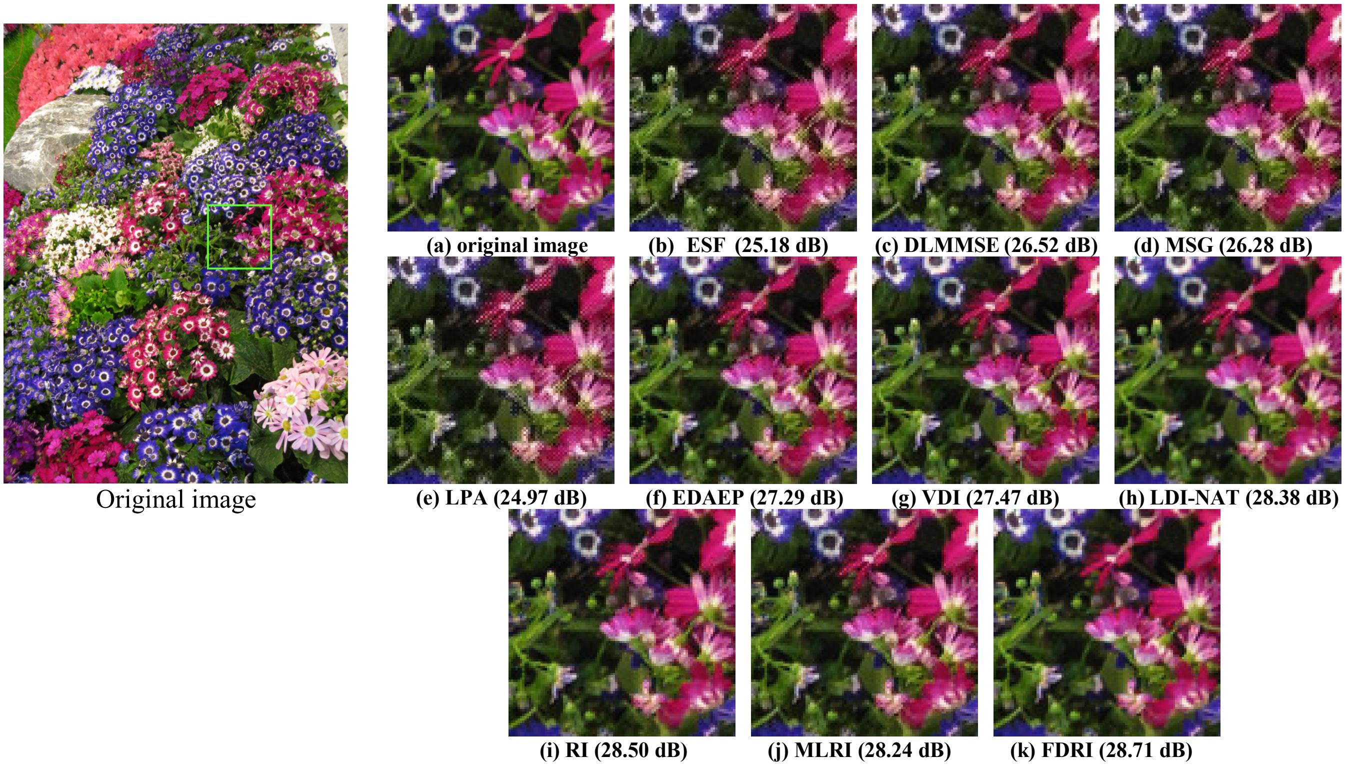

Original image

(a) original image (b) ESF (25.18 dB) (c) DLMMSE (26.52 dB) (d) MSG (26.28 dB)

(e) LPA (24.97 dB) (f) EDAEP (27.29 dB) (g) VDI (27.47 dB) (h) LDI-NAT (28.38 dB)

(i) RI (28.50 dB) (j) MLRI (28.24 dB) (k) FDRI (28.71 dB)

Fig. 9. Demosaicking results of a cropped region

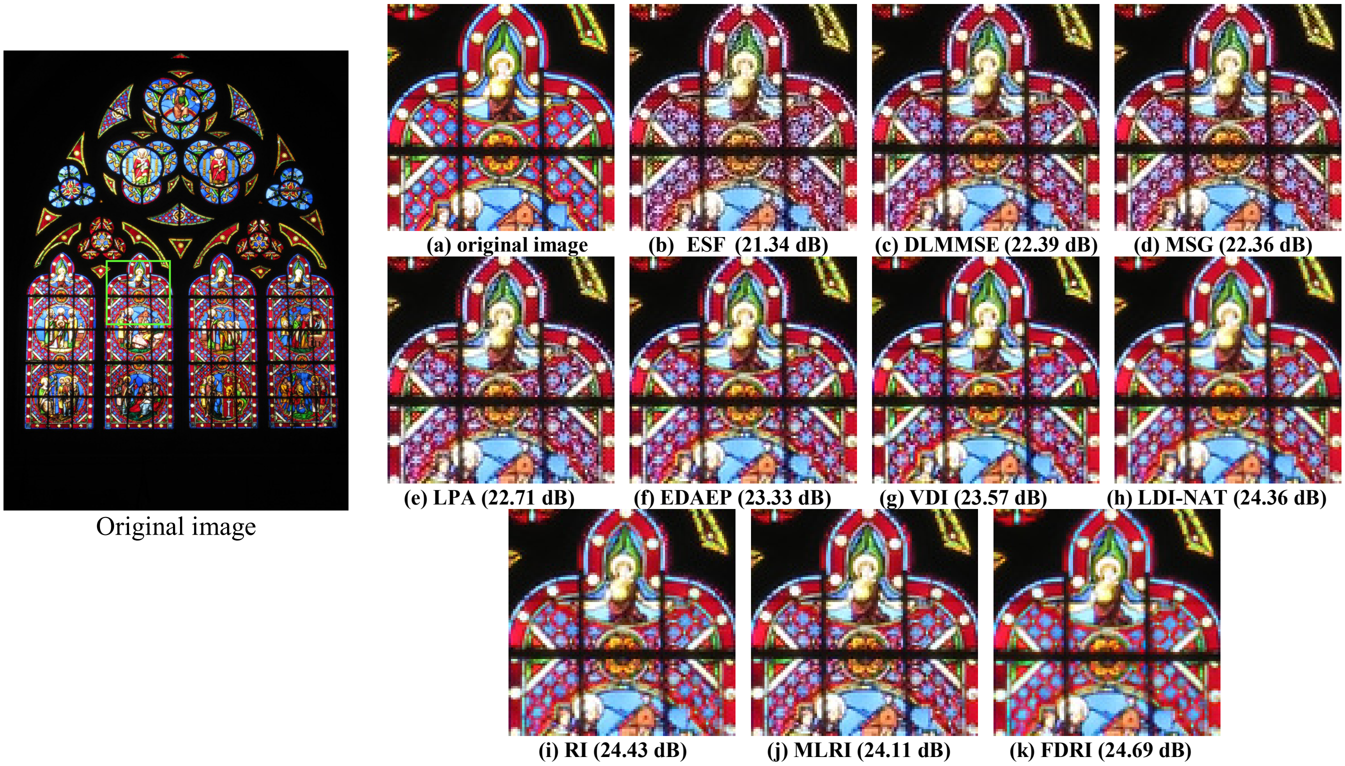

Original image

(a) original image (b) ESF (21.34 dB) (c) DLMMSE (22.39 dB) (d) MSG (22.36 dB)

(e) LPA (22.71 dB) (f) EDAEP (23.33 dB) (g) VDI (23.57 dB) (h) LDI-NAT (24.36 dB)

(i) RI (24.43 dB) (j) MLRI (24.11 dB) (k) FDRI (24.69 dB)

Fig. 10. Demosaicking results of a cropped region

number of guided filtering process compare with RI and MLRI, and also have smaller operations for residual calculation for the G channel interpolations. Guided filtering was a more time-intensive process than Laplacian filtering and residual calculating.

We compared computational complexity using CPU processing time. Each method's original source code from the respective authors was used to calculate the CPU processing

TABLE VI
AVERAGE COMPUTATIONAL TIME COMPARISON ON MCMASTER IMAGE (SEC)

ESF	DLMMSE	MSG	LPA	EDAEP	VDI	LDI-NAT	RI	MLRI	FDRI
5.9839	8.5878	5.5430	0.6528	0.2455	3.3062	519.8159	1.1582	1.5514	0.8125

time under the same test condition. As shown in Table VI, the proposed algorithm took 0.81 s per image; MLRI and RI respectively took 1.55 and 1.15 s per image. FDRI reduced the guided filtering and residual calculation processes. However, it required an additional Laplacian filtering process; therefore, FDRI showed lower complexity than MLRI and still consumed lower computation time than RI. LDI-NAT consumed more than 8 min in the same condition on account of the nonlocal mean method used to refine the interpolation. VDI took an average of 3.31 s per image. Based on the results, the proposed algorithm demonstrated a relatively low complexity burden.

V. CONCLUSION

In this paper, we proposed four direction residual interpolation. The proposed FDRI method improves residual interpolation by exploiting four directions and adopts a 5x5 Laplacian filter. From experimental results, the proposed *G* plane interpolation yielded a high performance gain; the developed method was applied to the McMaster dataset and LC images with great objective results. These results showed that the FDRI strategy can be very effective on images captured by a digital sensor. In addition, the subjective results demonstrated that FDRI successfully removed demosaicking artifacts, such as false coloring, and produced clean images.

REFERENCES

[1] B. E. Bayer, "Color imaging array," U.S. Patent 3 971 065, July 1976.

[2] B. K. Gunturk, J. Glotzbach, Y. Altunbasak, R. W. Schafer, and R.M. Mersereau, "Demosaicking: Color filter array interpolation," *IEEE Signal Process. Mag.*, vol. 22, no. 1, pp. 44–54, Jan. 2005.

[3] W. Lu and Y. Tan, "Color filter array demosaicking: new method and performance measures," *IEEE Trans. Image Processing,* vol. 12, no. 10, pp. 1194–1210, 2003.

[4] L. Zhang and X. Wu, "Color demosaicking via directional linear minimum mean square-error estimation," *IEEE Trans. Image Process.*,vol. 14, no. 12, pp. 2167–2178, Dec. 2005.

[5] D. Paliy, V. Katkovnik, R. Bilcu, S. Alenius, and K. Egiazarian,"Spatially adaptive color filter array interpolation for noiseless and noisydata," *Int. J. Imag. Syst. Technol*., vol. 17, no. 3, pp. 105–122, 2007.

[6] Z. Dengwen, S. Xiaoliu and D. Weiming, "Colour demosaicking with directional filtering and weighting," *IET Image Process.,* vol. 6, no. 8, pp. 1084–1092, Nov. 2012.

[7] D. Paliy, V. Katkovnik, R. Bilcu, S. Alenius, and K. Egiazarian, "Spatially adaptive color filter array interpolation for noiseless and noisy data," *Int. J. Imag. Syst. Technol.,* vol. 17, no. 3, pp. 105–122, 2007.

[8] C.A. Laroche and M.A. Prescott, Apparatus and method for adaptively interpolating a full color image utilizing chrominance gradients, U.S.Patent 5 373 322, Dec. 1994.

[9] H. S. Malvar, L.-W. He, and R. Cutler, High-quality linear interpolation for demosaicing of Bayer-patterned color images, in *Proc. Int. Conf. Acoust Speech Signal Process.*, 2004, pp. 485–488.

[10] X. Wu and N. Zhang, "Primary-consistent soft-decision color demosaicking for digital cameras," *IEEE Trans. Image Process.*, vol. 13, no. 1, pp. 1263–1274, Sep. 2004.

[11] D. Menon, S. Andriani, and G. Calvagno, "Demosaicing with directional filtering and a posteriori decision," *IEEE Trans. Image Process.*, vol. 16, no. 1, pp. 132–141, Jan. 2007.

[12] I. Pekkucuksen and Y. Altunbasak, "Edge strength filter based color filter array interpolation," *IEEE Trans. Image Process.*, vol. 21, no. 1, pp. 393-397, Jan. 2012.

[13] I. Pekkucuksen and Y. Altunbasak, "Multiscale Gradients-Based ColorFilter Array Interpolation," *IEEE Trans. Image Process.*, vol. 22, no. 1, pp. 157-165, Jan. 2013.

[14] X. Li, B. Gunturk, and L. Zhang, "Image demosaicing: a systematic survey," *in Proc. of SPIE*, vol. 6822, pp. 68221J, 2008.

[15] The Kodak color image dataset, *Image Available* [Online]. Available: http://r0k.us/graphics/kodak/.

[16] L. Zhang, A. Wu, A. Buades, and X. Li, "Color demosaicking by local directional interpolation and non-local adaptive thresholding," *Journal of Electronic Imaging*, vol. 20, no. 2, pp. 023016, 2011.

[17] W. Chen, P. Chang, "Effective demosaicking algorithm based on edge property for color filter arrays," *Digit. Signal Process.,* vol. 22, no. 1, pp. 163–169, Jan. 2012.

[18] X. Chen, G. Jeon, and J. Jeong, "Voting-based directional interpolation method and its application to still color image demosaicking," *IEEE Trans. Circuits Syst. Video Technol.*, vol. 24, no.2, pp. 255-262, Feb. 2014.

[19] D. Kiku, Y. Monno, M. Tanaka, and M. Okutomi, "Residual interpolation for color image demosaicking," *Proc. of IEEE Int. Conf. on Image Processing (ICIP)* , pp. 2304–2308, 2013.

[20] D. Kiku, Y. Monno, M. Tanaka, and M. Okutomi, "Minimized-Laplacian residual interpolation for color image demosaicking." *IS&T/SPIE Electronic Imaging*, pp. 90230L-1–90230L-6, 2014.

[21] J. F. Hamilton and J. E. Adams, "Adaptive color plane interpolation in single sensor color electronic camera," U.S. Patent 5 629 734, May. 1997.

[22] K. He, J. Sun, X. Tang, He, "Guided image filtering." *Computer Vision–ECCV 2010*, pp. 1-14, 2010.

[23] X. Zhang, "S-CIELAB: A spatial extension to the CIE *L*a*b** DeltaE color difference metric," Stanford Univ., Stanford, CA, 1998 [Online]. Available: http://white.stanford.edu/~brian/scielab/scielab.html

[24] The McMaster color image dataset, *Image Available* [Online]. Available: http://www4.comp.polyu.edu.hk/~cslzhang/CDM_Dataset.htm.

[25] L. Zhang, L, Zhang, X. Mou, and D. Zhang, "FSIM: a feature similarity index for image quality assessment," *IEEE Trans. Image Process.,* vol. 20, no. 8 pp. 2378–2386, Aug. 2011.

[26] L. Condat. (2010) *Image Available* [Online]. Available: http://www.gipsa-lab.grenoble-inp.fr/～laurent.condat/imagebase.html.

Yonghoon Kim received a B.S degree from the Department of Electronics and Computer Engineering from Hanyang University, Korea, in 2009. He is currently pursuing a Ph.D. degree in Electronic and Computer Engineering at Hanyang University. His research interests include motion estimation, intra prediction of video compression in H.264 and HEVC, and image processing, including demosaicing and denoising.

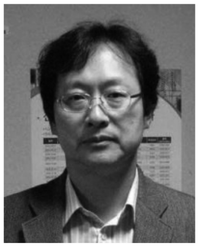

Jechang Jeong received a B.S. degree in electronic engineering from Seoul National University, Korea, in 1980, an M.S. degree in electrical engineering from the Korea Advanced Institute of Science and Technology in 1982, and a Ph.D. degree in electrical engineering from the University of Michigan, Ann Arbor, in 1990. From 1982 to 1986, he was with the

Korean Broadcasting System, where he helped develop teletext systems. From 1990 to 1991, he worked as a postdoctoral research associate at the University of Michigan, Ann Arbor, where he helped to develop various signal-processing algorithms. From 1991 through 1995, Dr. Jeong was with the Samsung Electronics Company, Korea, where he was involved in the development of HDTV, digital broadcasting receivers, and other multimedia systems. Since 1995, he has conducted research at Hanyang University, Seoul, Korea. His research interests include digital signal processing, digital communication, and image and audio compression for HDTV and multimedia applications. He has published numerous technical papers. Dr. Jeong received the Scientist of the Month Award in 1998 from the Ministry of Science and Technology of Korea, and he was the recipient of the 2007 IEEE Chester Sall Award and 2008 ETRI Journal Paper Award. He was also honored with a government commendation in 1998 from the Ministry of Information and Communication of Korea.